Heterogeneous expression of the SARS-Coronavirus-2 receptor ACE2 in the human respiratory tract

Miguel Ortiz Bezara[1], Andrew Thurman[2], Alejandro Pezzulo[2], Mariah R. Leidinger[3], Julia A. Klesney-Tait[2], Philip H. Karp[2], Ping Tan[2], Christine Wohlford-Lenane[1], Paul B. McCray, Jr.[1*], David K. Meyerholz[3*]

Departments of Pediatrics[1], Internal Medicine[2], and Pathology[3]; University of Iowa College of Medicine, University of Iowa, Iowa City, IA USA

*Contributed equally

Correspondence:

David K. Meyerholz (david-meyerholz@uiowa.edu)

Paul B. McCray, Jr. (paul-mccray@uiowa.edu)

Running title: Expression of ACE2 in the human respiratory tract

Impact: The mapping of ACE2, the receptor for SARS-CoV-2, to specific anatomical regions and to particular cell types in the human respiratory tract will help guide future studies and provide molecular targets for antiviral therapies. We saw no increase of receptor expression in the presence of known risk factors for severe coronavirus disease 2019.

Author contributions:

Conceptualization and writing – original draft, M.O.B., P.B.M. and D.K.M.; Data curation, A.T.; Formal analysis, M.O.B., A.T., A.P. and D.K.M.; Investigation, A.T., A.P., M.R.L., C.W.-L. and D.K.M.; Visualization, M.O.B., A.T., D.K.M.; Resources, A.P., J.A.K.-T., P.H.K., P.T., P.B.M. and D.K.M.; Writing – review and editing, M.O.B, A.T., A.P., M.R.L., J.A.K.-T., P.H.K., P.T., C.W.-L., P.B.M. and D.K.M

This work is supported by the National Institutes of Health (NIH) Grant P01 AI060699; and the Pathology Core, which are partially supported by the Center for Gene Therapy for Cystic Fibrosis (NIH Grant P30 DK-54759), and the Cystic Fibrosis Foundation. P.B.M. is supported by the Roy J. Carver Charitable Trust.

Abstract:

Rationale: Zoonotically transmitted coronaviruses are responsible for three disease outbreaks since 2002, including the current coronavirus disease 2019 pandemic, caused by SARS-CoV-2. Its efficient transmission and range of disease severity raise questions regarding the contributions of virus-receptor interactions. ACE2 is a host ectopeptidase and the cellular receptor for SARS-CoV-2. Receptor expression on the cell surface facilitates viral binding and entry. However, reports of the abundance and distribution of ACE2 expression in the respiratory tract are limited and conflicting. *Objectives:* To determine ACE2 expression in the human respiratory tract and its association with demographic and clinical characteristics. *Methods:* Here, we systematically examined human upper and lower respiratory tract cells using single-cell RNA sequencing and immunohistochemistry to determine where the receptor is expressed. *Measurements and main results:* Our results reveal that ACE2 expression is highest within the sinonasal cavity and pulmonary alveoli, sites of presumptive viral transmission and severe disease development, respectively. In the lung parenchyma where severe disease occurs, ACE2 was found on the apical surface of a small subset of alveolar type II cells. We saw no increase of receptor expression in the presence of known risk factors for severe coronavirus disease 2019. *Conclusions:* The mapping of ACE2 to specific anatomical regions and to particular cell types in the respiratory tract will help guide future studies and provide molecular targets for antiviral therapies.

Word count: 223

Key words: Lung, expression, alveolar type II cells, ciliated cells

58 **Main text:**

59 Angiotensin-converting enzyme 2 (ACE2) is the cellular receptor for both severe acute
60 respiratory syndrome coronavirus (SARS-CoV) and SARS-CoV-2 (1, 2). SARS-CoV caused a
61 pneumonia outbreak in 2002-2003 with a mortality rate of 9.6% and over 800 deaths worldwide
62 (3). SARS-CoV-2 is the etiologic agent of coronavirus disease 2019 (COVID-19) which was first
63 recognized in December 2019 and has now reached pandemic proportions (2, 4). SARS-CoV-2
64 infection can be fatal, with the risk for increased disease severity correlating with advanced age
65 and underlying comorbidities, while children and younger individuals have milder disease (5, 6).
66 These trends could reflect age-related differences in ACE2 distribution and expression in the
67 respiratory tract. Previous studies have variably shown ACE2 protein in the upper and lower
68 respiratory tract, but cellular localization and distribution in human lung tissues have been
69 inconsistent and contradictory (7-10) (Supplemental Table 1). *In vitro* studies demonstrate that
70 ACE2 is expressed at the apical membrane of polarized airway epithelia, where it permits viral
71 interaction and cell entry (10, 11). Here, we investigated the hypothesis that ACE2 expression
72 drives disease severity in susceptible patient populations through enhanced abundance or
73 distribution of ACE2 in different locations or cell types of the respiratory tract.

74

75 Severe COVID-19 is characterized by pneumonia and acute lung injury, so we first
76 assessed publicly available scRNA-seq data from distal lung biopsies (12) and evaluated ACE2
77 transcript abundance in specific cell types. In the alveoli, most ACE2 transcripts were in alveolar
78 type II (AT2) cells (89.5% of $ACE2^{+}$ cells) (Figure 1a), but specifically within a subset of these
79 cells (1.2% of AT2 cells) (Figure 1b, Supplemental Figure 1a-b). Next, we optimized and
80 validated ACE2 immunohistochemistry in extrapulmonary control tissues with high ACE2

81 expression (Supplemental Figure 2). We evaluated human lung tissues by immunohistochemistry
82 (Supplemental Table 2 and Supplemental Table 3). Alveoli exhibited apical ACE2 protein in a
83 small number (usually ~1% or less) of AT2 cells (Figure 1c), consistent with the results from
84 scRNA-seq. The identity of these cells was confirmed by co-staining for surfactant protein-C.
85 This $ACE2^+$ subset of AT2 cells was often observed within areas of alveolar collapse (Figures
86 1d-f), and these $ACE2^+$ cells were more plump and larger than $ACE2^-$ AT2 cells in the same
87 tissue section (Figure 1g). AT2 cells can hypertrophy and proliferate following alveolar injury as
88 they repopulate damaged alveolar type I (AT1) cells along the alveolar wall (13). Interestingly,
89 alveolar macrophages were negative for ACE2 protein staining by immunohistochemistry,
90 despite previous reports of ACE2 protein in these cells (Supplemental Table 1). The lack of
91 ACE2 expression in macrophages was also confirmed by scRNA-seq data that revealed ACE2
92 mRNA transcripts in only 0.1% of macrophages, monocytes, or dendritic cells (Supplemental
93 Figure 1a-b). The concordance between scRNA-seq and immunohistochemistry results provides
94 evidence that ACE2 in the alveoli is primarily expressed in a subset of AT2 cells and that
95 alveolar macrophages do not express ACE2.
96
97 Recent evidence indicates that proteases such as TMPRSS2 facilitate entry of SARS-
98 CoV-2 into $ACE2^+$ cells (14). We evaluated scRNA-seq data and observed that TMPRSS2 was
99 expressed in 35.5% of all AT2 cells (Figure 2a), and in 50.0% of $ACE2^+$ AT2 cells (Figure 2b).
100 Additionally, we observed colocalization of ACE2 and TMPRSS2 on the apical membrane of
101 AT2 cells (Figure 2c). These findings suggest that AT2 cells with apical ACE2 and TMPRSS2
102 could readily facilitate SARS-CoV-2 cellular infection and disease as seen in COVID-19
103 patients.

104

105 We next evaluated ACE2 in the conducting airways (trachea, bronchi, bronchioles). In
106 the trachea and bronchi, apical ACE2 was rare and limited to ciliated cells (Figure 1h), similar to
107 previous results in primary human airway epithelial cultures (11). In the submucosal glands of
108 large airways, occasional serous cells and vessels near the acini were positive for ACE2
109 (Supplemental Figures 3a-b). In bronchioles, ACE2 was regionally localized (Figures 1i-k).
110 These findings show nominal detection of ACE2, corresponding with the lack of primary airway
111 disease (e.g. bronchitis, etc.) seen in COVID-19 patients.

112

113 Detection of ACE2 protein has had contrasting variability reported between several small
114 studies (8, 10). In this larger study, we saw regional distribution of ACE2 protein varied between
115 donors. We detected ACE2 protein in surface epithelium of large airways in only 12% of
116 tracheal and 27% of bronchial tissues (Figure 3a). In the distal areas of the lung, ACE2 was more
117 common, with positive protein detection in 36% of bronchiolar and 59% of alveolar samples
118 (Figure 3a). A similar pattern of variable alveolar ACE2 was seen for mRNA transcripts in the
119 scRNA-seq data, where 50% of donors showed low expression in AT2 cells, and the other 50%
120 of donors showed high expression in the same cell type (Figure 3b). These findings suggest that
121 ACE2 expression can vary between different lung regions and between individuals. Despite the
122 heterogeneity of ACE2 detection between donors, 79% of subjects had positive ACE2 protein
123 staining in at least one tissue. Given the large variability observed, it is possible that sampling
124 limitations were responsible for the lack of ACE2 detection in the remaining 21% of donors.
125 Additionally, we acknowledge that ACE2 could be expressed at levels below the limits of
126 detection for scRNA-seq or immunohistochemistry.

127

128 Factors that could regulate ACE2 levels in the human lower respiratory tract include sex,
129 age, or presence of comorbidities. The ACE2 gene resides on the X chromosome and therefore
130 could be differentially regulated between males and females due to variable X-inactivation (15).
131 Male sex correlates with increased levels of circulating ACE2 (reviewed in (16)) and early
132 reports suggest males have increased COVID-19 severity (17). Advanced age and chronic
133 comorbidities such as diabetes, cardiovascular disease, and renal disease are also associated with
134 increased circulating ACE2 (reviewed in (16)), and these characteristics have also been
135 associated with increased severity of COVID-19 (6, 18).

136

137 To evaluate whether the spatial distribution and abundance of ACE2 protein in the lower
138 respiratory tract differed by age, sex, or presence of comorbidities, we scored tissues for ACE2
139 protein levels (Supplemental Table 2). In the cohort, neither age nor sex were associated with
140 ACE2 protein detection (using the median age as cut-off) (Figures 3c-d). Since recent studies of
141 COVID-19 infections suggested that young children may have reduced disease severity when
142 infected by SARS-CoV-2 (6, 19), we compared lung tissue samples from children <10 years of
143 age to those from older subjects (19-71 years of age) and found that ACE2 protein detection was
144 higher in this subset of young children (Figure 3e). To test whether ACE2 distribution was
145 affected by the presence of underlying diseases, we assessed the ACE2 localization pattern using
146 tissues from subjects with chronic comorbidities (asthma, cardiovascular disease, chronic
147 obstructive pulmonary disease, cystic fibrosis, diabetes, and smokers) and compared them to
148 controls (Supplemental Table 2). The control group was similar in age to the chronic disease
149 group (Figure 3f). We observed no significant differences between the two groups in ACE2

150 distribution, except for bronchioles, where ACE2 protein was reduced in the chronic disease
151 group (Figure 3g, Supplemental Figure 3c). These results show that ACE2 levels in the
152 respiratory tract did not increase in association with risk factors for severe COVID-19, such as
153 advanced age and underlying chronic comorbidities. Instead, we saw increased ACE2 detection
154 in children <10 years of age and in the small airways (bronchioles) of individuals without
155 chronic comorbidities in our cohort. We note that not finding changes in receptor expression for
156 SARS-CoV-2 is different from another severe coronavirus disease, MERS, where comorbidities
157 were observed to increase its receptor detection in respiratory tissues (20, 21).
158
159 Given the unexpected heterogeneity in the lower respiratory tract, we also investigated
160 ACE2 in the upper respiratory tract. We studied ACE2 gene expression using publicly available
161 scRNA-seq data from nasal brushing and nasal turbinate samples (22) and observed ACE2
162 mRNA transcripts in 2-6% of epithelial cells (Supplemental Figure 4a-d). We then studied nasal
163 biopsy tissues and found that ACE2 protein was detected in all tissue samples and, when present,
164 was seen exclusively on the apical surface of ciliated cells. Distribution varied regionally based
165 on the characteristics of the epithelium, with rare detection in thicker ciliated pseudostratified
166 epithelium, and more abundant expression in thinner epithelium (Figures 4a-g). Thinner
167 epithelial height is recognized in specific regions including the floor of the nasal cavity,
168 meatuses, and paranasal sinuses (23). Both, epithelial heterogeneity and undefined biopsy sites in
169 sinonasal cavity, limited direct comparisons between scRNA-seq results and protein staining.
170 Additionally, it is possible ACE2 protein cannot be detected in all cell types with ACE2 mRNA
171 due to low expression, rapid protein turnover, or post-transcriptional regulation. The sinonasal
172 cavity is an interface between the respiratory tract and the environment. High SARS-CoV-2

173 viral loads can be detected in nasal swabs from infected patients (24), consistent with our ACE2
174 expression data. This reservoir of $ACE2^+$ cells may facilitate the reported transmission from
175 individuals who have very mild or asymptomatic disease (25).
176
177 Through study of these respiratory tissues, we found that ACE2 protein was most
178 consistently detected in the sinonasal cavity and the alveoli. Expression of ACE2 in the nasal
179 cavity could explain the high transmissibility of SARS-CoV-2 and HCoV-NL63, a cold-related
180 coronavirus, which also uses ACE2 as a receptor. One mystery is why SARS-CoV, which also
181 uses ACE2, was apparently unable to easily transmit from human-to-human (26). Whether this
182 represents differences in the interactions of SARS-CoV and SARS-CoV-2 with co-receptors (27)
183 or other factors in the nasal cavity remains to be investigated. SARS-CoV and SARS-CoV-2
184 both replicate in the lungs (28, 29), consistent with the ACE2 distribution defined in this and
185 suggested by previous studies (9, 10). Most of the ACE2 expression in the lung was found in
186 AT2 cells, which are targets for SARS-CoV (30) and presumably SARS-CoV-2 (29). Given that
187 AT2 cells are critical for surfactant protein production and serve as progenitor cells for the AT1
188 cells, damage to these cells could contribute to acute lung injury (31), which is a common feature
189 of severe COVID-19 (5). Infection of AT2 cells could disrupt epithelial integrity leading to
190 alveolar edema, and facilitate viral spread to other epithelial cells or to $ACE2^+$ interstitial
191 cells/vessels for systemic virus dissemination, given that SARS-CoV-2 has been detected in
192 blood (32). Furthermore, cell-to-cell spread of coronaviruses after initial infection could also
193 occur via receptor-independent mechanisms related to the fusogenic properties of the S protein
194 (33). It is interesting that computerized tomography studies of early disease in people with

195 COVID-19 demonstrate patchy ground glass opacities in the peripheral and posterior lungs,
196 regions that are more susceptible to collapse (34).
197
198 The elevated detection of ACE2 protein in demographic pools with expected low risk for
199 severe COVID-19 was unexpected and suggests alternative explanations. First, the potential
200 relationship between ACE2 in the respiratory tract and severe COVID-19 is likely complex. On
201 one hand, more receptor availability could enhance viral entry into cells and worsen disease
202 outcomes; alternatively, ACE2 may play a protective role in acute lung injury (35-37) and
203 therefore could improve disease outcomes. Our data would support the latter and implicate a
204 dualistic role for ACE2 as both a viral receptor and a protective agent in acute lung injury.
205 Additionally, ACE2 exists in cell-associated and soluble forms (38). It is possible that greater
206 ACE2 expression could result in increased soluble ACE2 in respiratory secretions where it might
207 act as a decoy receptor and reduce virus entry (1, 39). Second, other factors such as TMPRSS2
208 expression might be more important in regulating disease severity. TMPRSS2 on the apical
209 membrane of AT2 cells might facilitate SARS-CoV-2 entry when ACE2 is rare or even below
210 the limit of detection in this study.
211
212 In summary, we find that ACE2 protein has heterogeneous expression in the respiratory
213 tract with higher ACE2 detection in the sinonasal epithelium and AT2 cells that correlates with
214 putative sites for transmission and severe disease, respectively. The small subset of $ACE2^{+}$ AT2
215 cells in the lung could be further studied to reveal factors regulating ACE2 expression and clarify
216 potential targets for antiviral therapies.
217 Word count: 2139
218

Acknowledgements:

We thank our laboratory members and colleagues Stanley Perlman, Robert Robinson, and Thomas Gallagher for their helpful discussion and technical assistance.

Competing interest declaration:

The authors declare no competing interests.

226 **Materials and methods:**

227

228 **Tissues:**

229 Studies on human tissues were approved by the institutional review board of the University of
230 Iowa. Tissues included nasal biopsies (n=3, deidentified and lacked evidence of significant
231 disease or cancer), lung donors, primary cell cultures (40), and autopsy tissues (control tissues)
232 that were selected from archival repositories as formalin-fixed paraffin-embedded blocks. Lung
233 cases were selected to comprise two case study groups: 1) Chronic disease group was defined as
234 having chronic comorbidities including: asthma, cardiovascular disease, chronic obstructive
235 pulmonary disease, cystic fibrosis, diabetes, and smoking. 2) Control group was defined as
236 lacking these chronic comorbidities and lacking clinical lung disease. The cumulative cohort
237 included 29 cases (15 chronic comorbidities and 14 controls) with a broad range of ages (0.5 –
238 71 years) and both sexes were represented (13 female and 16 male). For these lungs, if a trachea
239 or bronchus tissue block was available from the same case – these were included as well
240 (Supplemental Table 2). Bronchioles were observed in most lung sections and were defined as
241 intrapulmonary airways lacking evidence of cartilage or submucosal glands (41).

242

243 **Immunohistochemistry and immunofluorescence:**

244 All formalin-fixed paraffin-embedded tissues were sectioned (~4 μm) and hydrated through a
245 series of xylene and alcohol baths to water. Immunohistochemistry was then applied to these
246 studies to evaluate angiotensin-converting enzyme 2 (ACE2) (11), allograft inflammatory factor
247 1 (AIF1, also known as IBA1) (42), surfactant protein C (SP-C) (43) and mucin 5B (MUC5B)
248 (42). For more specifics about the reagents please see Supplemental Table 3.

249

250 For immunofluorescence, formalin-fixed and paraffin-embedded human lung blocks were
251 sectioned (~4 µm). Slides were baked (55°C x 15 min) and then deparaffinized (hydrated) in a
252 series of xylene and progressive alcohol baths. Antigen retrieval was performed using Antigen
253 Unmasking Solution (1:100, #H-3300) in citrate buffer (pH 6.0) solution to induce epitope
254 retrieval (5 min x 3 times) in the microwave. Slides were washed (PBS, 3 times, 5 min each) and
255 a PAP pen used to encircle the tissue. Slides were blocked with background blocking solution
256 (2% BSA in Superblock 1 hr in humid chamber). Primary antibodies anti-ACE2 (1:100, Mouse
257 monoclonal, MAB933, R&D Systems, Minneapolis, MN USA) and anti-TMPRSS2 (1:200,
258 Rabbit monoclonal, #ab92323, Abcam, Cambridge, MA USA) were diluted in blocking solution
259 (2% BSA in Superblock overnight 4°C). Secondary antibodies anti-mouse Alexa568 (for ACE2)
260 and anti-rabbit Alexa488 (for TMPRSS2) were applied at a concentration of 1:600 for 1 hour at
261 room temperature. Slides were washed and mounted with Vectashield containing DAPI.
262

263 **Tissue scoring:**

264 Stained tissue sections were examined for ACE2 localization using a post-examination method
265 for masking and scored by a masked pathologist following principles for reproducible tissue
266 scores (44). The initial examination showed a low incidence of ACE2 staining for various
267 tissues, so the following ordinal scoring system was employed to quantify number of staining-
268 positive cells: 0 = below the limit of detection; 1 = <1%; 2 = 1-33%; 3 = 34-66%; and 4 = >66%
269 of cells. For these anatomic regions (e.g. airway or alveoli), cell counts for each tissue were
270 made to know the population density per microscopic field to make reproducible interpretations.
271 For determination of AT2 cell size, ACE2 and SP-C protein immunostaining were evaluated on

272 the same lung tissue section for each case. A region of minimally diseased lung was examined
273 and SP-C$^+$ AT2 cells were measured for diameter in the plane perpendicular to the basement
274 membrane. Similar measurements were then made for ACE2$^+$/SP-C$^+$ cells.
275
276 **Analysis of single cell RNA sequencing data:**
277 Single cell RNA sequencing data sets were accessed from Gene Expression Omnibus (GEO)
278 series GSE121600 (22) and GSE122960 (12). For GSE121600, raw H5 files for bronchial biopsy
279 (GSM3439925), nasal brushing (GSM3439926), and turbinate (GSM3439927) samples were
280 downloaded, and barcodes with less than 1000 unique molecular identifiers (UMIs) were
281 discarded. For GSE122960, filtered H5 files for eight lung transplant donor samples from lung
282 parenchyma (GSM3489182, GSM3489185, GSM3489187, GSM3489189, GSM3489191,
283 GSM3489193, GSM3489195, GSM3489197) were downloaded, and all barcodes were retained.
284 The eight donors varied from 21-63 years of age (median age = 48) and were composed of five
285 African American, one Asian, and two white donors, and 2 active, 1 former, and 5 never
286 smokers. Gene count matrices from the eight donors were aggregated for analysis.
287
288 All four data sets (bronchial biopsy, nasal brushing, turbinate, and lung parenchyma) were
289 processed in a similar manner. Gene-by-barcode count matrices were normalized, log-
290 transformed, and scaled followed by dimension reduction using principal components analysis
291 (PCA). Principal components were used to obtain uniform manifold approximation and
292 projection (UMAP) visualizations, and cells were clustered using a shared nearest neighbor
293 (SNN) approach. Cell types associated with each cluster were identified by determining marker
294 genes for each cluster. All analyses were performed using R package Seurat version 3.1.1 (45).

295 In the nasal brushing sample, we were unable to associate a cell type with one cluster containing
296 776 cells (16.5%) due to low UMIs, so these cells were discarded. For the bronchial biopsy
297 sample, 82.4% of cells had less than 3,000 UMIs, so we lacked confidence in assigned cell types,
298 and thus results were not reported.
299
300 For the lung parenchyma data, gene expression in alveolar type II cells for a single donor was
301 quantified by summing up gene counts for all alveolar type II cells and dividing by total UMIs
302 for all alveolar type II cells to get normalized counts, followed by rescaling the normalized
303 counts to obtain counts per million (CPM).
304
305 **Statistical analyses:**
306 Statistical analyses for group comparisons and tissue scoring data were performed using
307 GraphPad Prism version 8 (GraphPad Software, La Jolla, CA USA). For group comparisons,
308 Mann Whitney U tests or T-tests were used for group comparisons as appropriate and Cochran-
309 Armitage test for trend was used to compare ACE2 protein detection in different tissues.
310

311 **References:**

312 1. Li W, Moore MJ, Vasilieva N, Sui J, Wong SK, Berne MA, Somasundaran M, Sullivan JL,
313 Luzuriaga K, Greenough TC, Choe H, Farzan M. Angiotensin-converting enzyme 2 is a
314 functional receptor for the SARS coronavirus. *Nature* 2003; 426: 450-454.
315 2. Zhou P, Yang XL, Wang XG, Hu B, Zhang L, Zhang W, Si HR, Zhu Y, Li B, Huang CL,
316 Chen HD, Chen J, Luo Y, Guo H, Jiang RD, Liu MQ, Chen Y, Shen XR, Wang X, Zheng
317 XS, Zhao K, Chen QJ, Deng F, Liu LL, Yan B, Zhan FX, Wang YY, Xiao GF, Shi ZL. A
318 pneumonia outbreak associated with a new coronavirus of probable bat origin. *Nature*
319 2020.
320 3. Lam CW, Chan MH, Wong CK. Severe acute respiratory syndrome: clinical and laboratory
321 manifestations. *Clin Biochem Rev* 2004; 25: 121-132.
322 4. Wilder-Smith A, Chiew CJ, Lee VJ. Can we contain the COVID-19 outbreak with the same
323 measures as for SARS? *Lancet Infect Dis* 2020.
324 5. Zhou F, Yu T, Du R, Fan G, Liu Y, Liu Z, Xiang J, Wang Y, Song B, Gu X, Guan L, Wei Y,
325 Li H, Wu X, Xu J, Tu S, Zhang Y, Chen H, Cao B. Clinical course and risk factors for
326 mortality of adult inpatients with COVID-19 in Wuhan, China: a retrospective cohort
327 study. *Lancet* 2020.
328 6. Guan WJ, Ni ZY, Hu Y, Liang WH, Ou CQ, He JX, Liu L, Shan H, Lei CL, Hui DSC, Du B,
329 Li LJ, Zeng G, Yuen KY, Chen RC, Tang CL, Wang T, Chen PY, Xiang J, Li SY, Wang
330 JL, Liang ZJ, Peng YX, Wei L, Liu Y, Hu YH, Peng P, Wang JM, Liu JY, Chen Z, Li G,
331 Zheng ZJ, Qiu SQ, Luo J, Ye CJ, Zhu SY, Zhong NS, China Medical Treatment Expert
332 Group for C. Clinical Characteristics of Coronavirus Disease 2019 in China. *N Engl J*
333 *Med* 2020.
334 7. Bertram S, Glowacka I, Muller MA, Lavender H, Gnirss K, Nehlmeier I, Niemeyer D, He Y,
335 Simmons G, Drosten C, Soilleux EJ, Jahn O, Steffen I, Pohlmann S. Cleavage and
336 activation of the severe acute respiratory syndrome coronavirus spike protein by human
337 airway trypsin-like protease. *J Virol* 2011; 85: 13363-13372.
338 8. Bertram S, Heurich A, Lavender H, Gierer S, Danisch S, Perin P, Lucas JM, Nelson PS,
339 Pohlmann S, Soilleux EJ. Influenza and SARS-coronavirus activating proteases
340 TMPRSS2 and HAT are expressed at multiple sites in human respiratory and
341 gastrointestinal tracts. *PLoS One* 2012; 7: e35876.
342 9. Hamming I, Timens W, Bulthuis ML, Lely AT, Navis G, van Goor H. Tissue distribution of
343 ACE2 protein, the functional receptor for SARS coronavirus. A first step in
344 understanding SARS pathogenesis. *J Pathol* 2004; 203: 631-637.
345 10. Ren X, Glende J, Al-Falah M, de Vries V, Schwegmann-Wessels C, Qu X, Tan L, Tschernig
346 T, Deng H, Naim HY, Herrler G. Analysis of ACE2 in polarized epithelial cells: surface
347 expression and function as receptor for severe acute respiratory syndrome-associated
348 coronavirus. *J Gen Virol* 2006; 87: 1691-1695.
349 11. Jia HP, Look DC, Shi L, Hickey M, Pewe L, Netland J, Farzan M, Wohlford-Lenane C,
350 Perlman S, McCray PB, Jr. ACE2 receptor expression and severe acute respiratory
351 syndrome coronavirus infection depend on differentiation of human airway epithelia. *J*
352 *Virol* 2005; 79: 14614-14621.
353 12. Reyfman PA, Walter JM, Joshi N, Anekalla KR, McQuattie-Pimentel AC, Chiu S, Fernandez
354 R, Akbarpour M, Chen CI, Ren Z, Verma R, Abdala-Valencia H, Nam K, Chi M, Han S,
355 Gonzalez-Gonzalez FJ, Soberanes S, Watanabe S, Williams KJN, Flozak AS, Nicholson

356 TT, Morgan VK, Winter DR, Hinchcliff M, Hrusch CL, Guzy RD, Bonham CA, Sperling
357 AI, Bag R, Hamanaka RB, Mutlu GM, Yeldandi AV, Marshall SA, Shilatifard A, Amaral
358 LAN, Perlman H, Sznajder JI, Argento AC, Gillespie CT, Dematte J, Jain M, Singer BD,
359 Ridge KM, Lam AP, Bharat A, Bhorade SM, Gottardi CJ, Budinger GRS, Misharin AV.
360 Single-Cell Transcriptomic Analysis of Human Lung Provides Insights into the
361 Pathobiology of Pulmonary Fibrosis. *Am J Respir Crit Care Med* 2019; 199: 1517-1536.
362 13. Olajuyin AM, Zhang X, Ji HL. Alveolar type 2 progenitor cells for lung injury repair. *Cell*
363 *Death Discov* 2019; 5: 63.
364 14. Hoffmann M, Kleine-Weber H, Schroeder S, Kruger N, Herrler T, Erichsen S, Schiergens
365 TS, Herrler G, Wu NH, Nitsche A, Muller MA, Drosten C, Pohlmann S. SARS-CoV-2
366 Cell Entry Depends on ACE2 and TMPRSS2 and Is Blocked by a Clinically Proven
367 Protease Inhibitor. *Cell* 2020.
368 15. Carrel L, Willard HF. X-inactivation profile reveals extensive variability in X-linked gene
369 expression in females. *Nature* 2005; 434: 400-404.
370 16. Anguiano L, Riera M, Pascual J, Soler MJ. Circulating ACE2 in Cardiovascular and Kidney
371 Diseases. *Curr Med Chem* 2017; 24: 3231-3241.
372 17. Mo P, Xing Y, Xiao Y, Deng L, Zhao Q, Wang H, Xiong Y, Cheng Z, Gao S, Liang K, Luo
373 M, Chen T, Song S, Ma Z, Chen X, Zheng R, Cao Q, Wang F, Zhang Y. Clinical
374 characteristics of refractory COVID-19 pneumonia in Wuhan, China. *Clin Infect Dis*
375 2020.
376 18. Lu Q, Shi Y. Coronavirus disease (COVID-19) and neonate: What neonatologist need to
377 know. *J Med Virol* 2020.
378 19. Dong Y, Mo X, Hu Y, Qi X, Jiang F, Jiang Z, Tong S. Epidemiological Characteristics of
379 2143 Pediatric Patients With 2019 Coronavirus Disease in China. *Pediatrics* 2020.
380 20. Meyerholz DK, Lambertz AM, McCray PB, Jr. Dipeptidyl Peptidase 4 Distribution in the
381 Human Respiratory Tract: Implications for the Middle East Respiratory Syndrome. *Am J*
382 *Pathol* 2016; 186: 78-86.
383 21. Seys LJM, Widagdo W, Verhamme FM, Kleinjan A, Janssens W, Joos GF, Bracke KR,
384 Haagmans BL, Brusselle GG. DPP4, the Middle East Respiratory Syndrome Coronavirus
385 Receptor, is Upregulated in Lungs of Smokers and Chronic Obstructive Pulmonary
386 Disease Patients. *Clin Infect Dis* 2018; 66: 45-53.
387 22. Ruiz Garcia S, Deprez M, Lebrigand K, Cavard A, Paquet A, Arguel MJ, Magnone V, Truchi
388 M, Caballero I, Leroy S, Marquette CH, Marcet B, Barbry P, Zaragosi LE. Novel
389 dynamics of human mucociliary differentiation revealed by single-cell RNA sequencing
390 of nasal epithelial cultures. *Development* 2019; 146.
391 23. Sternberg SS. Histology for Pathologists. Philadelphia, PA USA: Lippincott-Raven
392 Publishers; 1997.
393 24. Wang W, Xu Y, Gao R, Lu R, Han K, Wu G, Tan W. Detection of SARS-CoV-2 in Different
394 Types of Clinical Specimens. *JAMA* 2020.
395 25. Bai Y, Yao L, Wei T, Tian F, Jin DY, Chen L, Wang M. Presumed Asymptomatic Carrier
396 Transmission of COVID-19. *JAMA* 2020.
397 26. Wang Y, Wang Y, Chen Y, Qin Q. Unique epidemiological and clinical features of the
398 emerging 2019 novel coronavirus pneumonia (COVID-19) implicate special control
399 measures. *J Med Virol* 2020.

400 27. Wrapp D, Wang N, Corbett KS, Goldsmith JA, Hsieh CL, Abiona O, Graham BS, McLellan
401 JS. Cryo-EM structure of the 2019-nCoV spike in the prefusion conformation. *Science*
402 2020; 367: 1260-1263.
403 28. Yen YT, Liao F, Hsiao CH, Kao CL, Chen YC, Wu-Hsieh BA. Modeling the early events of
404 severe acute respiratory syndrome coronavirus infection in vitro. *J Virol* 2006; 80: 2684-
405 2693.
406 29. Zhang H, Zhou P, Wei Y, Yue H, Wang Y, Hu M, Zhang S, Cao T, Yang C, Li M, Guo G,
407 Chen X, Chen Y, Lei M, Liu H, Zhao J, Peng P, Wang CY, Du R. Histopathologic
408 Changes and SARS-CoV-2 Immunostaining in the Lung of a Patient With COVID-19.
409 *Ann Intern Med* 2020.
410 30. Mossel EC, Wang J, Jeffers S, Edeen KE, Wang S, Cosgrove GP, Funk CJ, Manzer R, Miura
411 TA, Pearson LD, Holmes KV, Mason RJ. SARS-CoV replicates in primary human
412 alveolar type II cell cultures but not in type I-like cells. *Virology* 2008; 372: 127-135.
413 31. Ware LB, Matthay MA. The acute respiratory distress syndrome. *N Engl J Med* 2000; 342:
414 1334-1349.
415 32. Chen W, Lan Y, Yuan X, Deng X, Li Y, Cai X, Li L, He R, Tan Y, Deng X, Gao M, Tang G,
416 Zhao L, Wang J, Fan Q, Wen C, Tong Y, Tang Y, Hu F, Li F, Tang X. Detectable 2019-
417 nCoV viral RNA in blood is a strong indicator for the further clinical severity. *Emerg*
418 *Microbes Infect* 2020; 9: 469-473.
419 33. Gallagher TM, Buchmeier MJ, Perlman S. Dissemination of MHV4 (strain JHM) infection
420 does not require specific coronavirus receptors. *Adv Exp Med Biol* 1993; 342: 279-284.
421 34. Song F, Shi N, Shan F, Zhang Z, Shen J, Lu H, Ling Y, Jiang Y, Shi Y. Emerging 2019
422 Novel Coronavirus (2019-nCoV) Pneumonia. *Radiology* 2020; 295: 210-217.
423 35. Gu H, Xie Z, Li T, Zhang S, Lai C, Zhu P, Wang K, Han L, Duan Y, Zhao Z, Yang X, Xing
424 L, Zhang P, Wang Z, Li R, Yu JJ, Wang X, Yang P. Angiotensin-converting enzyme 2
425 inhibits lung injury induced by respiratory syncytial virus. *Sci Rep* 2016; 6: 19840.
426 36. Imai Y, Kuba K, Rao S, Huan Y, Guo F, Guan B, Yang P, Sarao R, Wada T, Leong-Poi H,
427 Crackower MA, Fukamizu A, Hui CC, Hein L, Uhlig S, Slutsky AS, Jiang C, Penninger
428 JM. Angiotensin-converting enzyme 2 protects from severe acute lung failure. *Nature*
429 2005; 436: 112-116.
430 37. Zou Z, Yan Y, Shu Y, Gao R, Sun Y, Li X, Ju X, Liang Z, Liu Q, Zhao Y, Guo F, Bai T, Han
431 Z, Zhu J, Zhou H, Huang F, Li C, Lu H, Li N, Li D, Jin N, Penninger JM, Jiang C.
432 Angiotensin-converting enzyme 2 protects from lethal avian influenza A H5N1
433 infections. *Nat Commun* 2014; 5: 3594.
434 38. Lambert DW, Yarski M, Warner FJ, Thornhill P, Parkin ET, Smith AI, Hooper NM, Turner
435 AJ. Tumor necrosis factor-alpha convertase (ADAM17) mediates regulated ectodomain
436 shedding of the severe-acute respiratory syndrome-coronavirus (SARS-CoV) receptor,
437 angiotensin-converting enzyme-2 (ACE2). *J Biol Chem* 2005; 280: 30113-30119.
438 39. Hofmann H, Geier M, Marzi A, Krumbiegel M, Peipp M, Fey GH, Gramberg T, Pohlmann
439 S. Susceptibility to SARS coronavirus S protein-driven infection correlates with
440 expression of angiotensin converting enzyme 2 and infection can be blocked by soluble
441 receptor. *Biochem Biophys Res Commun* 2004; 319: 1216-1221.
442 40. Itani OA, Chen JH, Karp PH, Ernst S, Keshavjee S, Parekh K, Klesney-Tait J, Zabner J,
443 Welsh MJ. Human cystic fibrosis airway epithelia have reduced Cl- conductance but not
444 increased Na+ conductance. *Proc Natl Acad Sci U S A* 2011; 108: 10260-10265.

445 41. Meyerholz DK, Suarez CJ, Dintzis SM, Frevert CW. Comparative Anatomy and Histology:
446 A Mouse, Rat and Human Atlas. Academic Press - Elsevier; 2018.
447 42. Meyerholz DK, Lambertz AM, Reznikov LR, Ofori-Amanfo GK, Karp PH, McCray PB, Jr.,
448 Welsh MJ, Stoltz DA. Immunohistochemical Detection of Markers for Translational
449 Studies of Lung Disease in Pigs and Humans. *Toxicol Pathol* 2016; 44: 434-441.
450 43. Krishnamurthy S, Wohlford-Lenane C, Kandimalla S, Sartre G, Meyerholz DK, Theberge V,
451 Hallee S, Duperre AM, Del'Guidice T, Lepetit-Stoffaes JP, Barbeau X, Guay D, McCray
452 PB, Jr. Engineered amphiphilic peptides enable delivery of proteins and CRISPR-
453 associated nucleases to airway epithelia. *Nat Commun* 2019; 10: 4906.
454 44. Meyerholz DK, Beck AP. Principles and approaches for reproducible scoring of tissue stains
455 in research. *Lab Invest* 2018; 98: 844-855.
456 45. Stuart T, Butler A, Hoffman P, Hafemeister C, Papalexi E, Mauck WM, 3rd, Hao Y,
457 Stoeckius M, Smibert P, Satija R. Comprehensive Integration of Single-Cell Data. *Cell*
458 2019; 177: 1888-1902 e1821.
459

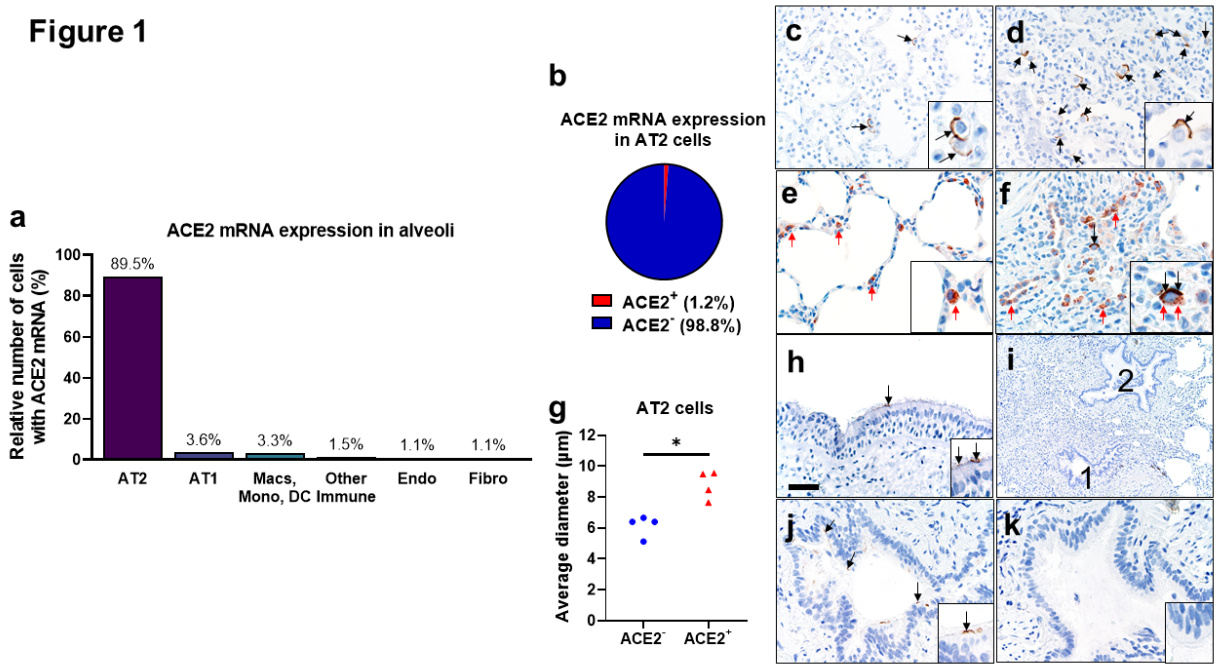

Figure 1. ACE2 expression in human lower respiratory tract. **a, b**) Single-cell RNA sequencing reanalysis of ACE2 expression in alveoli from lung parenchyma samples [14]. Airway cells (basal, mitotic, ciliated, club) are not shown. **a**) 89.5% of the cells expressing ACE2 mRNA in the alveoli are alveolar type II cells. **b**) Only 1.2% of alveolar type II cells express ACE2 mRNA. **c-f**, **h-k**) Detection of ACE2 protein (brown color, black arrows and insets) in representative sections of lower respiratory tract regions and tissue scoring (see Supplemental Table 2) (**g**). **c, d**) Alveolar regions had uncommon to regional polarized apical staining of solitary epithelial cells (**c**) that (when present) were more readily detected in collapsed regions of lung (**d**). **e, f**) SP-C (red arrows, inset) and ACE2 (black arrows, inset) dual immunohistochemistry on the same tissue sections. **e**) Non-collapsed regions had normal SP-C$^+$ AT2 cells lacking ACE2. **f**) Focal section of peri-airway remodeling and collapse with several SP-C$^+$ (red arrows) AT2 cells, but only a small subset of AT2 cells had prominent apical ACE2 protein (black arrows, inset). **g**) SP-C$^+$/ACE2$^+$ AT2 cells were often larger than SP-C$^+$/ACE2$^-$ AT2 cells from same lung sections (see also **d** and **e** insets) indicative of AT2 hypertrophy, each data point represents the average

475 value for each case from 5-10 cell measurements per group, P=0.0014, paired T-test. **h**) Large
476 airways (trachea and bronchi) exhibited rare ACE2 protein on the apical surface of ciliated cells.
477 **i-k**) Small airways (bronchioles) exhibited uncommon to localized apical ACE2 protein in
478 ciliated cells (**j**, #1 in **i**) while the adjacent bronchioles (**k**, #2 in **i**) lacked protein. AT2: alveolar
479 type II. AT1: alveolar type I. Macs: Macrophages. Mono: Monocytes. DC: dendritic cells. Other
480 immune cells: B cells, mast cells, natural killer/T cells. Endo: Endothelial. Fibro:
481 Fibroblasts/myofibroblasts. Bar = 35 (b-e, g), 140 (h) and 70 μm (i, j).
482

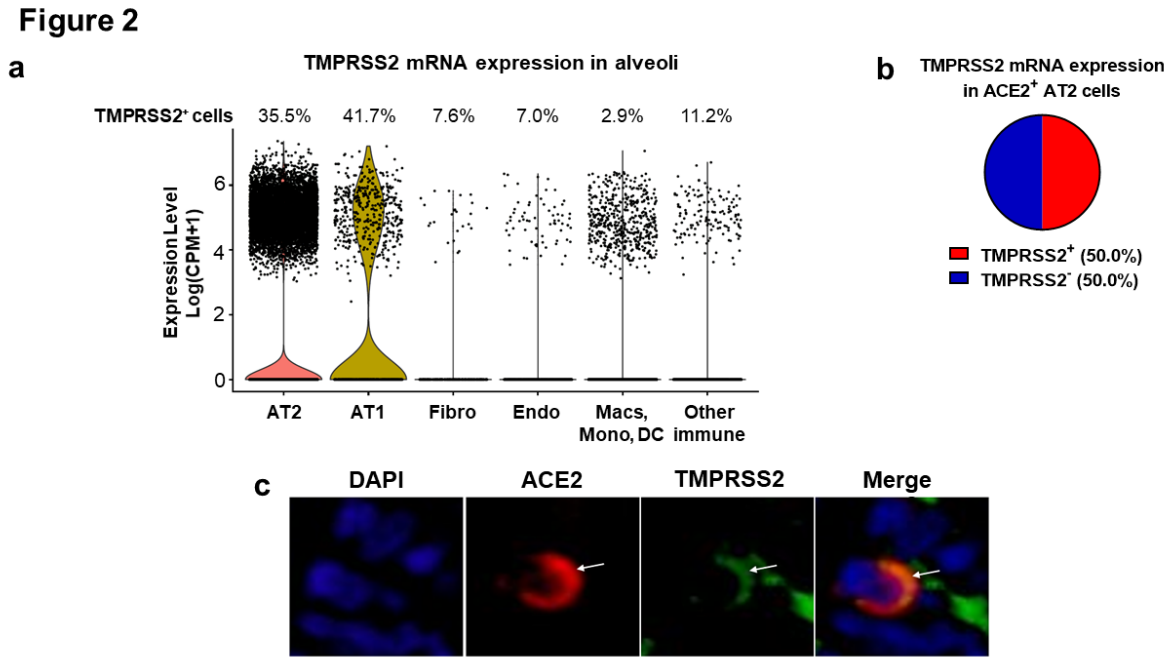

483

484 **Figure 2.** TMPRSS2 expression in the alveoli. **a, b**) Single-cell RNA sequencing reanalyses of
485 TMPRSS2 expression in alveoli from lung parenchyma [14]. **a**) Percentage of TMPRSS2^{+} cells
486 within each cell type shows TMPRSS2 transcripts in 35.5% of alveolar type II cells. Airway
487 cells (basal, mitotic, ciliated, club) are not shown. Violin plots represent expression, each data
488 point denotes a cell. **b**) TMPRSS2 expression in ACE2^{+} alveolar type II cells. **c**)
489 Immunofluorescence of alveoli shows apical colocalization of ACE2 and TMPRSS2 (white
490 arrows). AT2: alveolar type II. AT1: alveolar type I. Macs: Macrophages. Mono: Monocytes.
491 DC: dendritic cells. Other immune cells: B cells, mast cells, natural killer/T cells. Endo:
492 Endothelial. Fibro: Fibroblasts/myofibroblasts. CPM: counts per million.

493

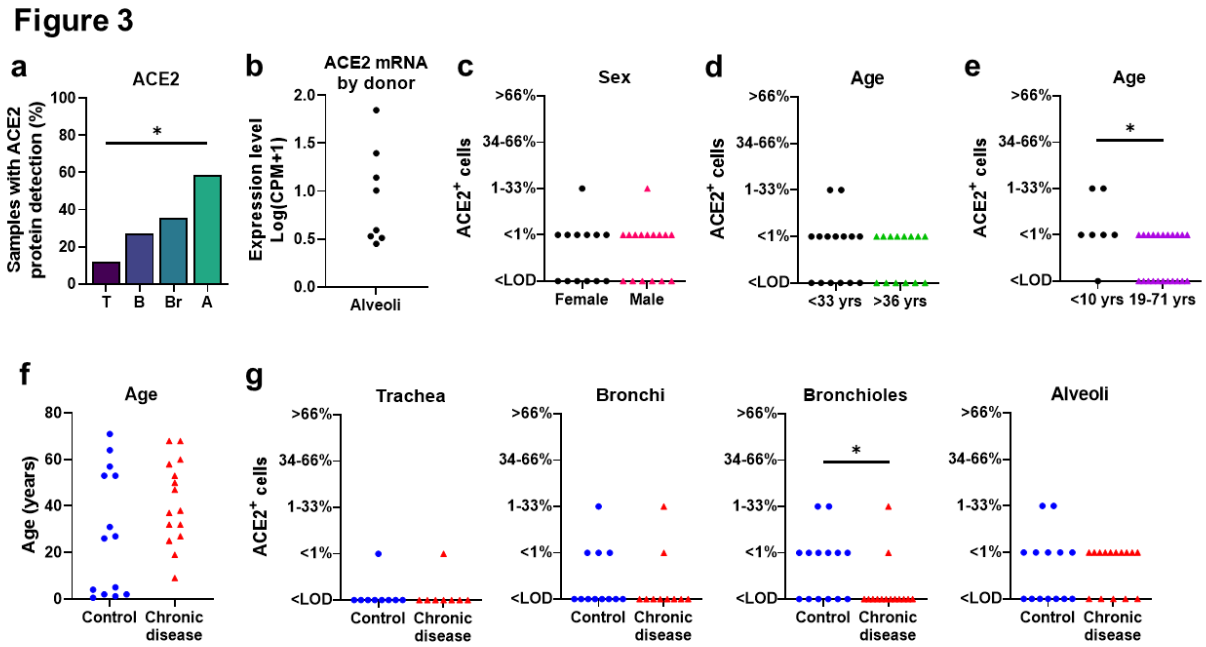

494

495 **Figure 3.** ACE2 localization and scores in respiratory tissues. **a**) ACE2 protein had progressively
496 increased detection between donors in tissues from trachea (T), bronchi (B), bronchioles (Br), to
497 alveoli (A), (P=0.0009, Cochran-Armitage test for trend). **b**) ACE2 mRNA expression in the
498 alveoli varied between donors. **c-d**) ACE2 protein scores from lung samples showed no
499 differences based on sex or lower vs. upper ages (using median age as a cut-off) (A, P=0.7338
500 and B, P=0.7053, Mann-Whitney U test). **e**) ACE2 protein scores were elevated in young
501 children (<10 yrs) compared to the remaining subjects (19-71 yrs) (P=0.0282 Mann-Whitney U
502 test). **f**) Control and chronic disease groups did not have any significant differences in age
503 (P=0.1362 Mann-Whitney U test). **g**) ACE2 protein scores for trachea, bronchi, bronchiole, and
504 alveoli in control versus chronic disease groups (P= >0.9999, 0.6263, 0.0433, and 0.7359,
505 respectively, Mann-Whitney U test). CPM: counts per million. LOD: Limit of detection.

506

Figure 4

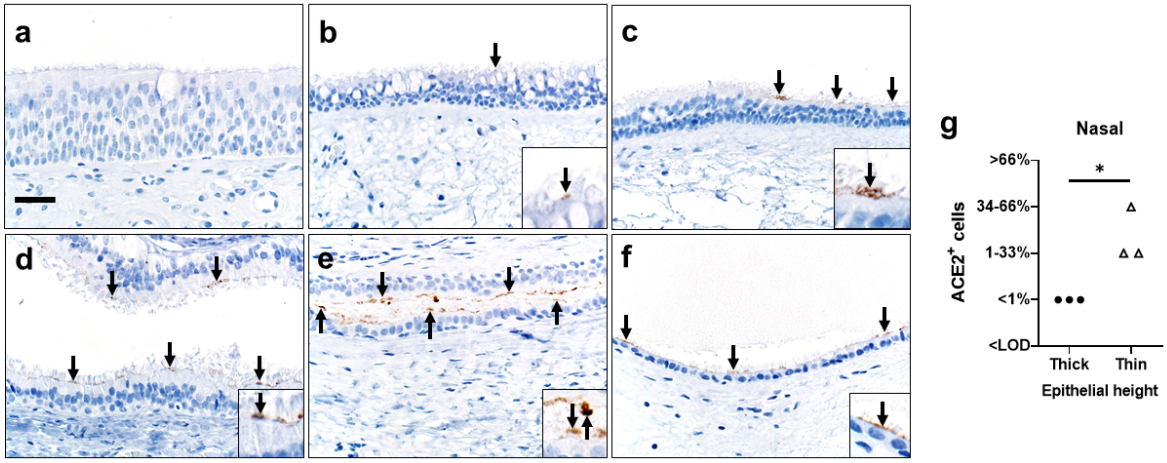

507

508 **Figure 4.** Detection of ACE2 protein (brown color, arrows and insets, **a-f**) and tissue scoring (**g**)
509 in representative sections of nasal tissues. **a, b**) In thick pseudostratified epithelium (PSE) ACE2
510 protein was absent (**a**) to rare (**b**) and apically located on ciliated cells. **c**) Tissue section shows a
511 transition zone from thick (left side, > ~4 nuclei) to thin (right side, ≤ ~4 nuclei) PSE and ACE2
512 protein was restricted to the apical surface of the thin PSE. **d-f**) ACE2 protein was detected
513 multifocally on the apical surface of ciliated cells in varying types of thin PSE, even to simple
514 cuboidal epithelium (**f**). Bar = 30 µm. **g**) ACE2 protein detection scores for each subject were
515 higher in thin than thick epithelium, (P=0.05, Mann-Whitney U test). LOD: Limit of detection.

516

517 **Supplemental information:**

Supplemental Figure 1

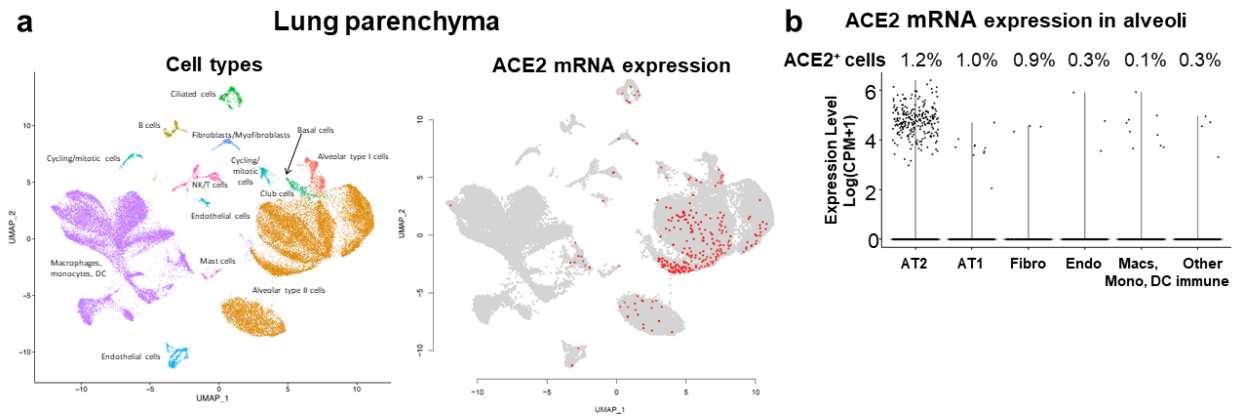

518

519 **Supplemental Figure 1.** Single-cell RNA sequencing reanalyses of ACE2 expression in lung
520 parenchyma [14]. **a**) Uniform manifold approximation and projection (UMAP) visualizations. Cells
521 were clustered using a shared nearest neighbor (SNN) approach. Cell types associated with each
522 cluster were identified by determining marker genes for each cluster. Each data point denotes a
523 cell. On the right panel, cells expressing ACE2 are shown in red. **b**) Violin plots representing
524 ACE2 expression in the alveoli. Airway cells (basal, mitotic, ciliated, club) are not shown.
525 Percentage of $ACE2^+$ cells within each cell type shows ACE2 transcripts in 1.2% of alveolar
526 type II cells and in 0.1% of macrophages, monocytes, or dendritic cells. Each data point denotes
527 a cell, most cells have no expression (0). AT2: alveolar type II. AT1: alveolar type I. Macs:
528 Macrophages. Mono: Monocytes. DC: dendritic cells. Other immune cells: B cells, mast cells,
529 natural killer/T cells. Endo: Endothelial. Fibro: Fibroblasts/myofibroblasts. NK: Natural killer.
530 CPM: Counts per million.

531

Supplemental Figure 2

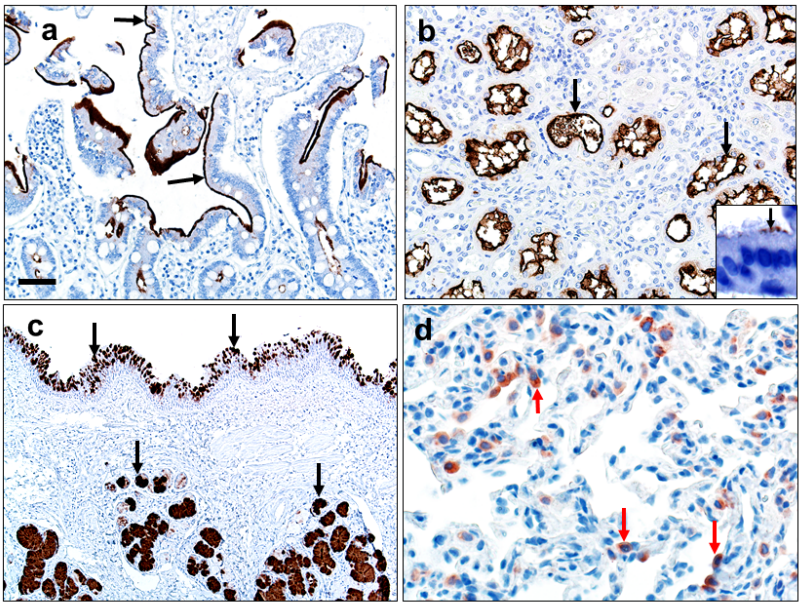

532

533 **Supplemental Figure 2.** Quality controls for ACE2 immunohistochemistry technique (**a, b**) and
534 tissue quality (**c, d**). **a, b**) ACE2 protein (brown color, black arrows) was detected along the
535 apical surface of small intestine enterocytes (**a**), renal tubule epithelium (**b**), and ciliated cells (**b,**
536 **inset**) of primary airway cell cultures. These findings demonstrate specific detection of ACE2
537 protein in cells/tissues consistent with known ACE2 expression. **c**) Representative
538 immunostaining of bronchus detected abundant MUC5B protein (brown color, black arrows) in
539 mucous cells of surface epithelium (top) and submucosal glands (bottom). **d**) Representative
540 sections of alveoli had SP-C^+ alveolar type II cells (red color, red arrows). These results (**c, d**)
541 demonstrate the tissues were intact and that immunostaining can be used to detect native airway
542 (**c**) and lung (**d**) proteins. Bar = 40 (a, b), 80 (c), and 20 µm (d).

543

Supplemental Figure 3

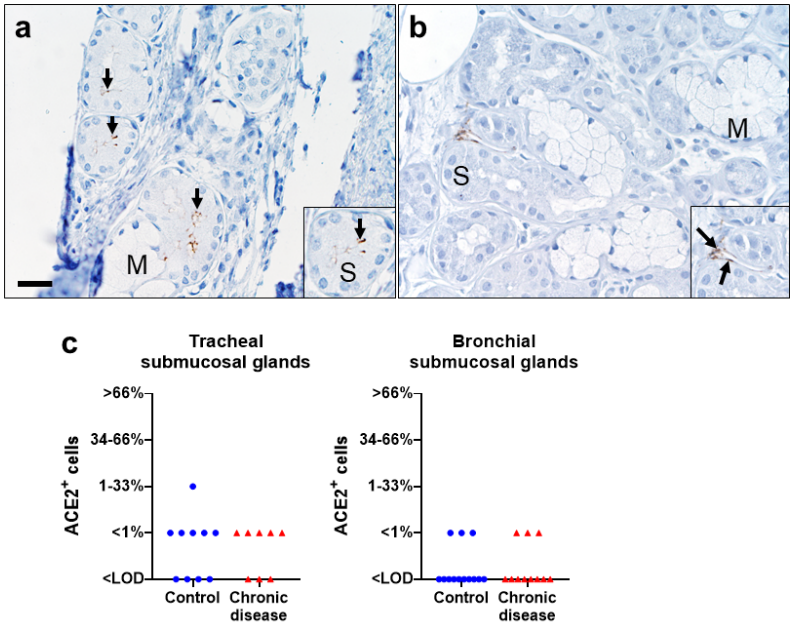

544

545 **Supplemental Figure 3.** Representative tissue section from submucosa of large airways
546 (trachea/bronchi) showing ACE2 protein localization (brown color, black arrows) (**a, b**) and
547 scores (**c**). **a**) Submucosal glands had uncommon to localized apical ACE2 protein (arrows) in
548 serous (S) cells, but not mucous (M) cells. **b**) Submucosal glands also had absent to uncommon
549 ACE2 protein (arrows) in the interstitium that centered on vascular walls and endothelium. This
550 vascular staining was uncommonly seen in lung too and corresponded to the low levels seen
551 transcripts for these endothelial cells (Supplemental Figure 1A-B). Note the absence of ACE2
552 staining in serous (S) or mucous (M) cells of the gland (**b**). **c**) ACE2 protein scores for each
553 subject for serous cells in submucosal glands from trachea and bronchi, in control versus chronic
554 disease groups (P>0.9999, 0.9999, respectively, Mann-Whitney U test). Bar = 25 μm. LOD:
555 Limit of detection.

556

Supplemental Figure 4

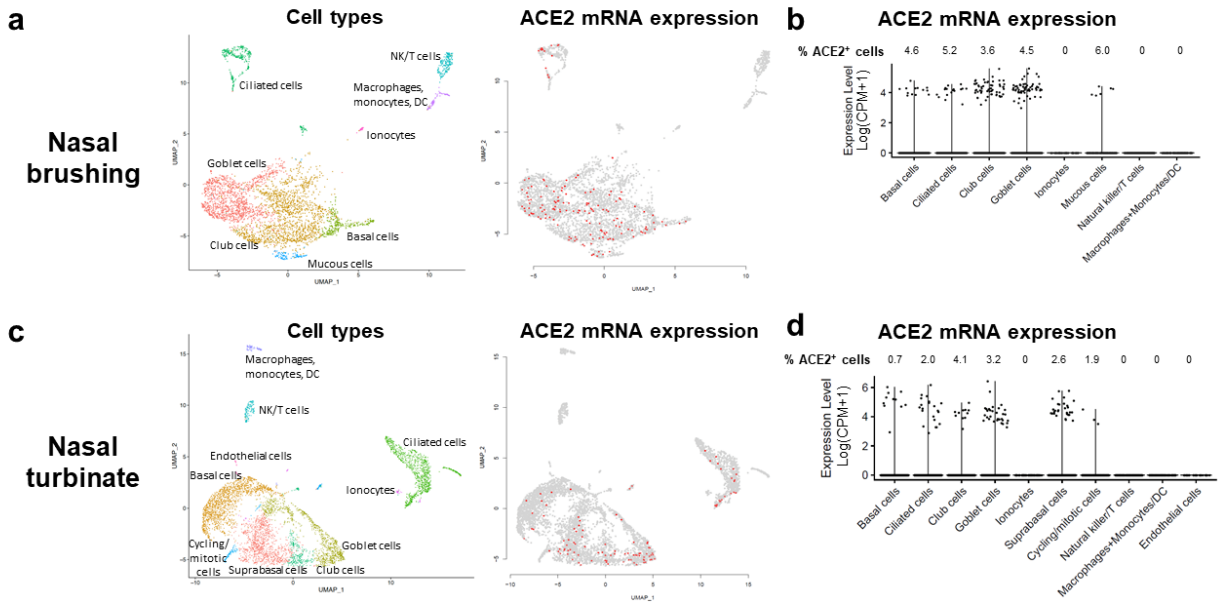

Supplemental Figure 4. Single-cell RNA sequencing reanalyses of ACE2 expression in nasal brushing (**a, b**) and nasal turbinate (**c, d**) [14]. **a, c**) Uniform manifold approximation and projection (UMAP) visualizations. Cells were clustered using a shared nearest neighbor (SNN) approach. Cell types associated with each cluster were identified by determining marker genes for each cluster. Each data point denotes a cell. On the right panels, cells expressing ACE2 are shown in red. **b, d**) Violin plots representing ACE2 expression. In nasal turbinate and nasal brushing, percentage of $ACE2^+$ cells within each cell type shows ACE2 expression on epithelial cells. Each data point denotes a cell, most cells have no expression (0). DC: dendritic cells. NK: Natural killer. CPM: Counts per million.

568 **Supplemental Table 1. ACE2 protein reported in surface epithelium (SE) of human**

569 **respiratory tract surface epithelium.**

Reported Cases (n)	Primary Ab	SN	T	B	Br	Al	Summary comments
Non-diseased lungs / nasal (5 each); diseased lungs (5) [12]	Polyclonal	SE (C++, basal cells in squamous epithelium)	n.d.	SE (C+)	n.d.	AT1 (C++); AT2 (C++)	Abundant ACE2 protein in lung epithelia
Non-diseased lungs (5) [13]	Undefined	n.d.	SE (C+, A+)	SE (C+, A+)	n.d.	"Alveoli" (A+) Mac (A+)	ACE2 is present on epithelia in several parts of the respiratory tract and macrophages
Lung (undefined) [10]	Polyclonal	n.d.	n.d.	SE (C+, N+, M+)	n.d.	AT1− AT2 (N+)	ACE2 is present in bronchial epithelium, AT2 cells and macrophages
Sinus (undefined) and Lung (undefined, same tissues as above) [11]	Polyclonal	SE (N++)	SE (−)	SE (C+, N++)	n.d.	AT1− AT2 (N++)	ACE2 is present in sinus and bronchial epithelium, AT2 cells and macrophages

570

571 Non-diseased: The cause of death was not directly related to lung disease

572 n.d.: Not described

573 Tissues: Sinonasal (SN), trachea (T), bronchi (B), bronchioles (Br), and alveoli (Al)

574 Cellular localization: cytoplasmic (C), nuclear (N), apical membrane (A)

575 Cells: Surface epithelium (SE), alveolar type I cells (AT1), alveolar type II cells (AT2), alveolar

576 macrophages (Mac)

577 ACE2 protein (based on published reports/figures): negative (−), weak (+), moderate to abundant

578 (++)

579

580 **Supplemental Table 2. Donor demographics and ACE2 distribution scores for each tissue**

581 **region.**

Case #	Group	Age (yrs)	Sex	Comorbidities	Trachea	Bronchi	Bronchioles	Alveoli
1	Control	5	F	Trauma	NA	2	2	1
2	Control	57	M	Arrhythmia	0	0	0	1
3	Control	31	M	Stroke (Joubert syndrome)	1	1	0	0
4	Control	53	F	Trauma	NA	0	0	1
5	Control	2	M	Brain hemorrhage	0	0	0	1
6	Control	2	M	Trauma	0	0	1	2
7	Control	0.5	M	Spinomuscular atrophy	NA	0	1	0
8	Control	71	M	Stroke, Parkinson's disease, nonsmoker	0	1	1	0
9	Control	4	F	Trauma	0	0	0	2
10	Control	1.2	M	Trauma	0	NA	1	1
11	Control	53	F	Trauma, nonsmoker	0	0	2	0
12	Control	26	F	NA	0	NA	0	0
13	Control	27	F	NA	NA	0	1	0
14	Control	64	M	NA	NA	1	1	0
15	Chronic disease	53	F	Smoker	0	NA	0	1
16	Chronic disease	60	M	COPD, smoker	NA	NA	0	1
17	Chronic disease	32	M	COPD, smoker	0	0	0	1
18	Chronic disease	68	M	COPD	NA	1	0	1
19	Chronic disease	68	F	COPD	NA	NA	1	1
20	Chronic disease	9	M	Asthma	0	0	0	1
21	Chronic disease	25	F	Cystic fibrosis	NA	0	0	0
22	Chronic disease	47	F	Cardiovascular disease	1	2	2	1
23	Chronic disease	27	M	Cystic fibrosis	0	NA	NA	1
24	Chronic disease	50	F	Cardiovascular disease, diabetes, asthma	NA	0	0	0
25	Chronic disease	37	M	Drug use, smoker	0	0	0	0
26	Chronic disease	38	M	Asthma (status asthmaticus)	0	0	0	0
27	Chronic disease	32	M	Cystic fibrosis	NA	NA	0	1
28	Chronic disease	58	F	Cardiovascular disease, diabetes, NASH	0	0	0	1
29	Chronic disease	19	F	Cystic fibrosis	NA	0	0	0

582

583 NA: Not available for analyses / COPD: Chronic obstructive pulmonary disease / NASH: Non-

584 alcoholic steatohepatitis.

585 Scoring: 0 = below limit of immunohistochemical detection; 1 = rare (<1%); 2 = <33%; 3 = 34-

586 66%; 4 = >66% of cells.

587

588 **Supplemental Table 3. Parameters for immunohistochemistry on fixed tissues.**

Target	Primary Antibody	Antigen Retrieval	Secondary Reagents
Allograft Inflammatory Factor 1 (AIF1)	Anti-AIF1 polyclonal (#019-19741, Wako Pure Chemical Industries, Ltd., Richmond, VA USA) in diluent 1:1000 x 1 hour	HIER, Citrate buffer pH 6.0, 110˚C for 15 min; 20 min cool down (Decloaking Chamber Plus, Biocare Medical, Concord, CA USA)	Dako EnVision+ System-HRP Labeled Polymer Anti-rabbit, 30 min (Dako North America, Inc., Carpentaria, CA USA) AEC chromogen, counterstain.
Angiotensin-Converting Enzyme 2 (ACE2)	Anti-ACE2, monoclonal (MAB933, R&D Systems, Minneapolis, MN USA) in diluent at 1:100 x 1 hour.	HIER, Citrate Buffer, pH 6.0, 110˚C for 15 minutes; 20 min cool down (Decloaking Chamber Plus, Biocare Medical, Concord, CA USA)	Dako EnVision+ System-HRP Labeled Polymer Anti-mouse, 60 min (Dako North America, Inc., Carpentaria, CA USA), DAB Chromogen, counterstain.
MUC5B	Rabbit anti-MUC5B polyclonal, (LSBio #LS-B8121, LifeSpan BioSciences, Inc., Seattle, WA) in Dako Antibody Diluent (Dako North America, Inc., Carpentaria, CA); 1:60,0000/30 min	HIER, Citrate buffer pH 6.0, 110˚C for 15min; 20 min cool down	Step 1: Biotinylated anti-Rabbit IgG (H+L) (Vector Laboratories, Inc., Burlingame, CA) in Dako Wash Buffer (Dako North America, Inc., Carpentaria, CA); 1:500, 30 min Step 2: Vectastain ABC Kit (Vector Laboratories, Inc., Burlingame, CA), 30min. DAB Chromogen, counterstain.
Surfactant Protein – C (SP-C)	Anti-SP-C, polyclonal (PA5-71680, Thermo Fisher Scientific, Waltham, MA USA) in diluent 1:100 x 1 hour	HIER, Citrate Buffer, pH 6.0, 110˚C for 15 minutes; 20 min cool down (Decloaking Chamber Plus, Biocare Medical, Concord, CA USA)	Dako EnVision+ System-HRP Labeled Polymer Anti-rabbit, 60 min (Dako North America, Inc., Carpentaria, CA USA), AEC chromogen, counterstain.

589

590 HIER – Heat-induced epitope retrieval

591 DAB – 3,3'-Diaminobenzidine (produces brown stain)

592 AEC - aminoethyl carbazole (produces red stain)

593 Counterstain – Harris hematoxylin (blue color)